

Phase Diagram and Quantum Order by Disorder in the Kitaev $K_1 - K_2$ Honeycomb Magnet

Ioannis Rousochatzakis,¹ Johannes Reuther,^{2,3} Ronny Thomale,⁴ Stephan Rachel,⁵ and N. B. Perkins¹¹*School of Physics and Astronomy, University of Minnesota, Minneapolis, Minnesota 55455, USA*²*Dahlem Center for Complex Quantum Systems and Fachbereich Physik, Freie Universität Berlin, 14195 Berlin, Germany*³*Helmholtz-Zentrum Berlin für Materialien und Energie, 14109 Berlin, Germany*⁴*Institute for Theoretical Physics, University of Würzburg, 97074 Würzburg, Germany*⁵*Institute for Theoretical Physics, Technische Universität Dresden, 01062 Dresden, Germany*

(Received 30 June 2015; revised manuscript received 27 August 2015; published 1 December 2015)

We show that the topological Kitaev spin liquid on the honeycomb lattice is extremely fragile against the second-neighbor Kitaev coupling K_2 , which has recently been shown to be the dominant perturbation away from the nearest-neighbor model in iridate Na_2IrO_3 , and may also play a role in $\alpha\text{-RuCl}_3$ and Li_2IrO_3 . This coupling naturally explains the zigzag ordering (without introducing unrealistically large longer-range Heisenberg exchange terms) and the special entanglement between real and spin space observed recently in Na_2IrO_3 . Moreover, the minimal $K_1 - K_2$ model that we present here holds the unique property that the classical and quantum phase diagrams and their respective order-by-disorder mechanisms are qualitatively different due to the fundamentally different symmetries of the classical and quantum counterparts.

DOI: 10.1103/PhysRevX.5.041035

Subject Areas: Condensed Matter Physics

I. INTRODUCTION

The search for novel quantum states of matter arising from the interplay of strong electronic correlations, spin-orbit coupling (SOC), and crystal field splitting has recently gained strong impetus in the context of $4d$ and $5d$ transition metal oxides [1]. The layered iridates of the A_2IrO_3 ($\text{A} = \text{Na}, \text{Li}$) family [2–7] have been at the center of this search because of the prediction [8,9] that the dominant interactions in these magnets constitute the celebrated Kitaev model on the honeycomb lattice, one of the few exactly solvable models hosting gapped and gapless quantum spin liquids (QSLs) [10]. This aspect together with the realization that the Kitaev spin liquid is stable with respect to moderate Heisenberg-like perturbations [9,11] has triggered a lot of experimental activity on A_2IrO_3 and, more recently, on the similar $\alpha\text{-RuCl}_3$ compound [12–14].

In the layered A_2IrO_3 magnets, the single-ion ground-state configuration of Ir^{4+} is an effective pseudospin $J_{\text{eff}} = 1/2$ doublet, where spin and orbital angular momenta are intertwined due to the strong SOC. In the original Kitaev-Heisenberg model proposed by Jackeli and Khaliullin [8], the pseudospins couple via two competing nearest-neighbor (NN) interactions: an isotropic antiferromagnetic (AFM) Heisenberg exchange J_1 and a highly anisotropic Kitaev interaction K_1 , which is strong and ferromagnetic (FM), a fact that is also

confirmed by *ab initio* quantum chemistry calculations by Katukuri and co-workers [15,16]. Nevertheless, neither Na_2IrO_3 nor Li_2IrO_3 are found to be in the spin-liquid state at low temperatures. Instead, they show, respectively, AFM zigzag and incommensurate long-range magnetic orders, none of which are actually present in the Kitaev-Heisenberg model for FM K_1 coupling.

The most natural way to obtain these magnetic states is by including further-neighbor Heisenberg couplings [15–18], which are non-negligible due to the extended nature of the

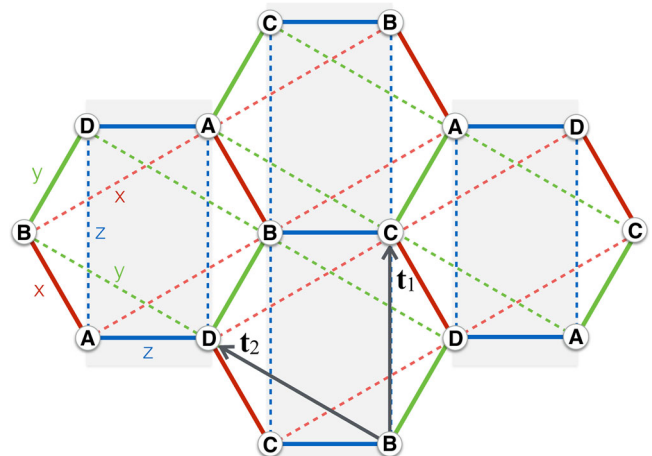


FIG. 1. The Kitaev $K_1 - K_2$ model with three types of NN (solid) and NNN (dashed) Ising bonds. Here, $\mathbf{t}_1 = a\mathbf{y}$ and $\mathbf{t}_2 = [-(\sqrt{3}/2)\mathbf{x} + (1/2)\mathbf{y}]a$ are two primitive translations and a is a lattice constant. We also show the vertical 2-leg ladders (shaded strips) discussed in the text, and the four-sublattice decomposition (A–D) related to the operations H_{yz} and H_{xyz} ; see text.

Published by the American Physical Society under the terms of the Creative Commons Attribution 3.0 License. Further distribution of this work must maintain attribution to the author(s) and the published article's title, journal citation, and DOI.

$5d$ orbitals of Ir^{4+} ions [6,19]. In addition, recent calculations by Sizyuk *et al.* [20] based on the *ab initio* density-functional data of Foyevtsova *et al.* [21] have shown that, for Na_2IrO_3 , the next-nearest-neighbor (NNN) exchange paths must also give rise to an anisotropic, Kitaev-like coupling K_2 , which turns out to be AFM. More importantly, this coupling is the largest interaction after K_1 . It has also been argued [22] that K_2 plays an important role in the stabilization of the incommensurate spiral state in Li_2IrO_3 and might be deduced from the strong-coupling limit of the Hubbard model with topological band structure [23,24].

Recent structural [12] and magnetic [13] studies have shown that the layered honeycomb magnet $\alpha\text{-RuCl}_3$ is another example of a strong SOC Mott insulator, where the Ru^{3+} ions are again described by effective $J_{\text{eff}} = 1/2$ doublets. At low T , this magnet exhibits zigzag ordering as in Na_2IrO_3 . Furthermore, the superexchange derivations [25,26] based on the *ab initio* tight-binding parameters show that the NNN coupling K_2 is again appreciable, and the signs of both K_1 and K_2 are reversed compared to Na_2IrO_3 (i.e., K_1 is AFM and K_2 is FM). However, a strong off-diagonal symmetric NN exchange Γ term [15,16,27], which is allowed by symmetry, is also present [25,26], together with a much smaller J_1 coupling. This compound must then be examined in connection to Γ , K_2 , and J_1 , since the Γ term alone is not sufficient to explain the experimental situation, as we discuss at length in Sec. VII.

Motivated by these studies, here we consider the minimal extension of the NN Kitaev model that incorporates the effect of K_2 , the $K_1 - K_2$ model. We show that an extremely weak K_2 is enough to stabilize the zigzag phases relevant for Na_2IrO_3 and $\alpha\text{-RuCl}_3$, without introducing large, second- and third-neighbor Heisenberg exchange J_2 and J_3 . While J_2 and J_3 are present in these compounds, the key point is that the Kitaev spin liquid is significantly more fragile against K_2 than J_2 and J_3 . Thus, in conjunction with the above predictions from superexchange derivations, our findings suggest that any adequate minimal model of these compounds should include the NNN coupling K_2 .

A very striking aspect of the zigzag phases (shared by all magnetic phases) of the $K_1 - K_2$ model is that they are stabilized only for quantum spins and not for classical spins, despite having a strong classical character. Indeed, these phases are Ising-like (with spins pointing along one of the three cubic axes), they are protected by a large excitation gap in the interacting $1/S$ spin-wave spectrum, and the spin lengths are extremely close to their classical value of $1/2$. Yet, these phases cannot be stabilized in the classical limit, in stark contrast to the conventional situation where quantum and thermal fluctuations work in parallel and often lead to the same order-by-disorder phenomena. Instead, this rare situation we encounter here stems from the manifestly different symmetry structure of the classical and quantum Hamiltonians and the underlying principle that time reversal can only act globally in quantum systems

(see below). This aspect has important ramifications for the phase diagram at zero and finite temperatures T .

II. MODEL AND PHASE DIAGRAM

The model we consider here is described by the effective spin-1/2 Hamiltonian

$$\mathcal{H} = K_1 \sum_{\langle ij \rangle} S_i^{\gamma_{ij}} S_j^{\gamma_{ij}} + K_2 \sum_{\langle\langle ij \rangle\rangle} S_i^{\lambda_{ij}} S_j^{\lambda_{ij}}, \quad (1)$$

where $\langle ij \rangle$ ($\langle\langle ij \rangle\rangle$) label NN (NNN) spins on the honeycomb lattice, S_j^a defines the a th Cartesian component of the spin operator at site j , and γ_{ij} (λ_{ij}) define the type of Ising coupling for the bond (ij); see Fig. 1. This model interpolates between two well-known limits, the exactly solvable Kitaev spin liquid [10] at $K_2 = 0$ and the triangular Kitaev model at $K_1 = 0$ [28–32]. It is easy to see that a finite K_2 ruins the exact solvability of the NN Kitaev model because the flux operators [10], $W_p = 2^6 S_1^z S_2^x S_3^y S_4^z S_5^y S_6^z$ (see site-labeling convention in Fig. 5, top left), around hexagons p are no longer conserved.

In the following, we parametrize $K_1 = \cos\psi$ and $K_2 = \sin\psi$, and take $\psi \in [0, 2\pi)$. It turns out that the physics actually remains the same under a simultaneous sign change of K_1 and K_2 , because this can be gauged

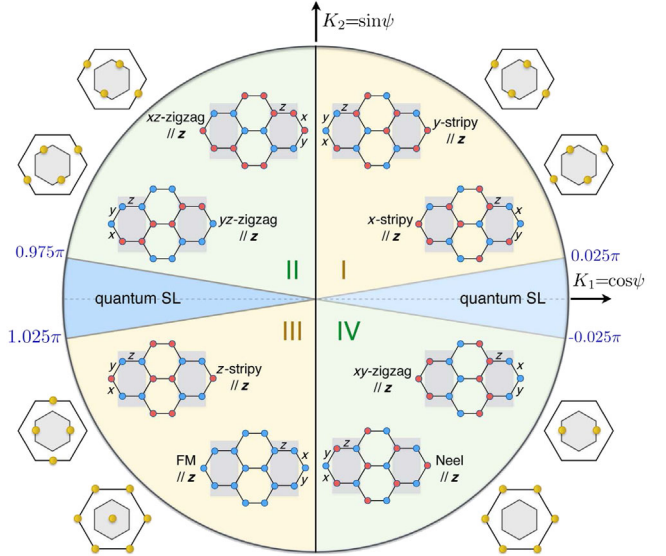


FIG. 2. The $T = 0$ phase diagram of the model Eq. (1) as found by exact diagonalizations. Each of the magnetic regions (I–IV) hosts 12 degenerate quantum states. Here, we show two members [where spins point along the z axis, blue (red) circles denote spin-up (spin-down)] that are related to each other by flipping the spins in every second ladder (shaded strips) of Fig. 1. The Bragg peaks corresponding to $\langle S_i^z S_j^z \rangle$ correlations are also shown in the extended Brillouin zone (assuming the same magnetic form factor in the two unit cell sublattices). The corresponding Bragg reflections for $\langle S_i^x S_j^x \rangle$ and $\langle S_i^y S_j^y \rangle$ are related to $\langle S_i^z S_j^z \rangle$ by \hat{C}_{6v} spin-orbit rotations [35].

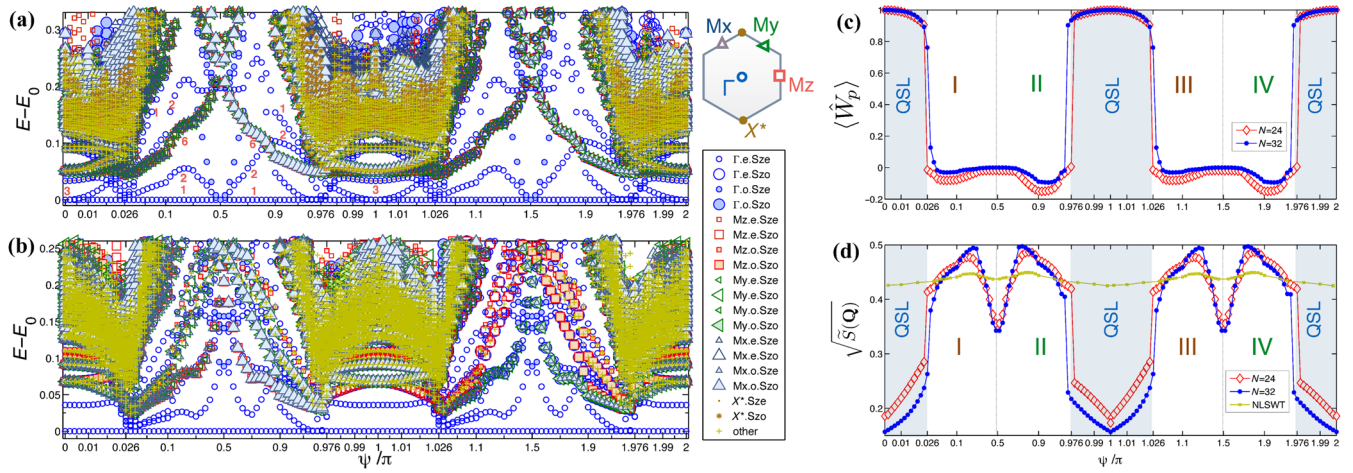


FIG. 3. (a),(b) Exact low-energy spectra (measured from the ground state energy E_0) of the 24-site (a) and 32-site (b) clusters, defined, respectively [35], by the spanning vectors $(2\mathbf{t}_1 - 4\mathbf{t}_2, 4\mathbf{t}_1 - 2\mathbf{t}_2)$ and $(2\mathbf{t}_1 - 4\mathbf{t}_2, 4\mathbf{t}_1)$. A nonlinear \mathbf{x} axis is used in order to highlight all regions of interest equally. The states are labeled by momenta \mathbf{k} in the first BZ, parity (“e” for even, “o” for odd) under inversion through hexagon centers, and parity under global spin π rotations around the x axis (“Sze” for even, “Szo” for odd). The (red) numbers in (a) denote the multiplicity of the lowest five levels in regions I and II and the ground state degeneracy at $\psi = 0$ and π . (c) ground state expectation value $\langle W_p \rangle$ of Kitaev’s flux operators. (d) Square root of the “symmetrized” ground state spin structure factor $\tilde{S}(\mathbf{Q})$ (see text), along with the spin length calculated from a self-consistent nonlinear spin-wave theory (NLSWT).

away by an operation $H_{yzx} = \prod_{i \in B} C_{2y}(i) \prod_{j \in C} C_{2z}(j) \prod_{k \in D} C_{2x}(k)$, which is the product of π rotations around the \mathbf{y} , \mathbf{z} , and \mathbf{x} axis, respectively, for the B, C, and D sublattices of Fig. 1. This *hidden* duality is a very common feature in many spin-orbital models [9,33,34] but does not exist when Heisenberg couplings are also present (in contrast to the symmetry H_{xyz} discussed below). Here, it reduces our study to the first two quadrants of the unit circle of ψ .

Figure 2 shows the quantum phase diagram as found by exact diagonalizations (ED) on finite clusters, see discussion below and numerical data shown in Fig. 3. There are six different regimes as a function of the angle ψ : the two QSLs (which have been enlarged for better visibility) around the exactly solvable Kitaev points ($\psi = 0$ and π) and four long-range magnetic regions (I–IV), hosting FM, Neel, stripy, and the zigzag phases that are relevant for Na_2IrO_3 (II) and $\alpha\text{-RuCl}_3$ (IV). Under the duality transformation H_{yzx} , the two QSLs map to each other, I maps to III and II maps to IV.

Each of the magnetic regions actually hosts twelve degenerate quantum states, some of which are even qualitatively different among themselves, with very distinct Bragg reflections. For example, the region III hosts six FM and six stripy AFM ground states, and IV hosts six Néel and six zigzag AFM ground states. This striking aspect stems from a non-global symmetry, H_{xyz} , which is the product of π -rotations around the x , y , and z axis, respectively, for the B, C, and D sublattices of Fig. 1. The two states shown in each magnetic region of Fig. 2 are related to each other by this symmetry, which for these particular states amounts to flipping the z -component of the spins in every second shaded ladder of Fig. 1. The

remaining ten states of the quantum ground state manifold arise by applying the global symmetries of the model: (i) the double cover \tilde{C}_{6v} of C_{6v} , and (ii) the double cover \tilde{D}_2 of the D_2 group of global π rotations in spin space.

Let us now turn to the numerical spectra shown in Figs. 3(a,b). First, the QSL regions are extremely narrow: They survive in a tiny window of $\delta\psi = 0.05\pi$ around the exact Kitaev points, which is confirmed by the comparison of ED against large scale pseudofermion functional renormalization group (PFFRG) calculations [36–39]. So the QSLs are extremely fragile against K_2 .

Second, Figs. 3(a,b) show very dense spectral features in the QSL regions, reflecting the continuum structure of fractionalized excitations above the Kitaev spin liquid. More specifically, for finite systems the GS degeneracy at the exact Kitaev points [40] is lifted by K_2 . Still, for small enough $|K_2|$, the QSLs must be gapless in the thermodynamic limit, because K_2 respects time reversal symmetry and is therefore not expected [10] to open a gap in the Majorana spectrum [42].

Third, unlike the QSL regions, the low-energy spectrum inside the magnetic regions is very discrete. In addition, most of the low-lying states within the energy window shown in Figs. 3(a,b) correspond precisely to the twelve quantum ground states discussed above. For finite systems, these states are admixed by a finite tunneling, leading to twelve symmetric eigenstates with quantum numbers corresponding to the decomposition of the symmetry broken states. This decomposition is worked out in detail in Ref. [35] and is indeed fully consistent with the ED data. So the lowest twelve states in each magnetic region of Figs. 3(a,b) will collapse to zero energy in the

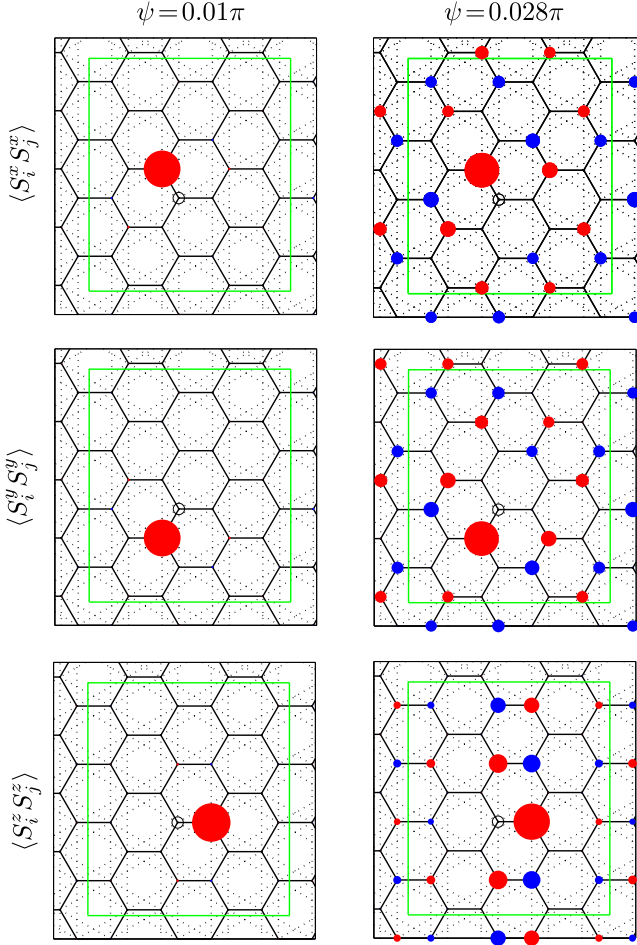


FIG. 4. Real-space spin-spin correlation profiles evaluated at the ground state of the $N = 32$ cluster, inside the first QSL phase ($\psi = 0.01\pi$, left-hand column) and inside the magnetic phase I ($\psi = 0.028\pi$, right-hand column). Different rows correspond to the three different channels $\langle S_i^\alpha S_j^\alpha \rangle$, $\alpha = x, y$, and z . The reference site i is indicated by the small black open circle. Positive (negative) correlations are shown by filled blue (filled red) circles, whose radius scales with the magnitude of the correlation. The difference between $\alpha = z$ and $\alpha = x, y$ stems from the fact that the 32-site cluster does not have the full point-group symmetry of the infinite lattice, and the momentum point \mathbf{M}_z is not equivalent by symmetry to \mathbf{M}_x and \mathbf{M}_y ; see Ref. [35].

thermodynamic limit, leaving the true magnon excitations with a large anisotropy gap (modulo finite size corrections), reflecting the anisotropic, Ising-like character of the magnetic model.

Fourth, the magnetic instabilities, which serve as good examples of deconfinement-confinement transitions [43–46] for the underlying spinons, are of first order, as they are accompanied by finite, abrupt changes [47] in several ground state properties, e.g., in $\langle W_p \rangle$, and in the spin-spin correlations. Specifically, at $\psi = 0$ and π , all fluxes W_p have a value of +1 [10]. A finite K_2 admixes sectors of different W_p , and so $\langle W_p \rangle$ drops continuously as we depart from the exact Kitaev’s points, until it jumps to

very low absolute values when we enter the magnetic phases; see Fig. 3(c).

Turning to the spin-spin correlations, their abrupt change at the transition can be seen in the behavior of the “symmetrized” spin structure factor $\tilde{S}(\mathbf{Q})$ shown in Fig. 3(d), which is defined as

$$\tilde{S}(\mathbf{Q}) = \frac{2}{N} \sum_{\alpha} \sum_{\mathbf{r} \neq 0} e^{i\mathbf{Q}^{(\alpha)} \cdot \mathbf{r}} \langle S_0^\alpha S_{\mathbf{r}}^\alpha \rangle, \quad (2)$$

where N is the number of sites, $\mathbf{Q}^{(\alpha)}$ is the ordering wave vector (see below) of the α th component of the spins ($\alpha = x, y, z$), and the extra factor of 2 in this definition accounts for the fact [35] that, for finite systems, there are no correlations between NN ladders like the ones shaded in Fig. 1, due to the nonglobal symmetry H_{xyz} discussed above. These data show clearly the short-range (long-range) character of spin-spin correlations inside (outside) the QSL regions.

This aspect can be seen more directly in Fig. 4, which shows the real-space spin-spin correlation profiles $\langle S_i^\alpha S_j^\alpha \rangle$, in the three channels $\alpha = x, y, z$, as calculated in the ground state of the 32-site cluster, inside the first QSL phase and slightly outside (magnetic phase I). The results show clearly the ultrashort-range nature of the correlations inside the QSL region and the long-range nature outside.

Finally, the spin-spin correlation profiles demonstrate the special anisotropic character of the correlations, whereby different spin components α are correlated along different directions of the lattice (or, equivalently, different spin components α order at different ordering wave vectors $\mathbf{Q}^{(\alpha)}$, see also Fig. 2), reflecting the locking between spin and orbital degrees of freedom in this model. Similar behavior is found for all other magnetic phases, including the zigzag phases that are relevant for Na_2IrO_3 and $\alpha\text{-RuCl}_3$. Such a signature of directional-dependent Kitaev couplings is exactly what has been reported recently by Chun *et al.* for Na_2IrO_3 [7]; see also last paragraph of Sec. VII.

In the following we shall probe the physical origin of the magnetic instabilities by taking one step back and examining the classical limit first.

III. CLASSICAL LIMIT

For classical spins, the frustration introduced by the K_2 coupling is different from the one of the pure K_1 model studied by Baskaran *et al.* [48]. A straightforward classical minimization in momentum space [35] gives lines of energy minima instead of a whole branch of minima [48], suggesting a subextensive ground state manifold structure, in analogy to compasslike models [49] or other special frustrated antiferromagnets [50].

We can construct one class of ground states by satisfying one of the three types of Ising bonds. We can choose, for example, the horizontal zz bonds and align the spins along the \mathbf{z} axis with relative orientations dictated by the signs

of K_1 and K_2 . The energy of the resulting configuration saturates the lower-energy bound [35], $E_b/(NS^2) = -|K_2| - |K_1|/2$, and is therefore one of the ground states. We can then generate other ground states by noting that K_1 and K_2 fix the relative signs of the spin projections S_z only within the vertical 2-leg ladders of the lattice (shaded strips in Fig. 1), but do not fix the relative orientation between different ladders, because these couple only via xx and yy Ising interactions which drop out at the mean-field level. This freedom leads to $2^{n_{\text{lad}}}$ ground states, where $n_{\text{lad}} \propto \sqrt{N}$ is the number of vertical ladders. This subextensive degeneracy stems from the presence of nonglobal, *sliding* operations [49,51–53] of flipping $S_z \mapsto -S_z$ for all spins belonging to one vertical ladder. Similarly, we can saturate the xx or the yy bonds, leading to 2-leg ladders running along the diagonal directions of the lattice. In total, this procedure delivers $3 \times 2^{n_{\text{lad}}}$ classical ground states.

These states are actually connected in parameter space by valleys formed by other, continuous families of ground states that can be generated by global $\text{SO}(3)$ rotations of the discrete states [35]. The degeneracy associated with these valleys is accidental and can therefore be lifted by fluctuations. This is in fact the situation at finite T where thermal fluctuations select one of the three types of discrete ground states, thereby breaking the threefold symmetry of the model in the combined spin-orbit space. This corresponds to a finite- T nematic phase where spins point along one of the three cubic axes but still sample all of the $2^{n_{\text{lad}}}$ corresponding states, without any long-range magnetic order. To achieve the latter, one needs to spontaneously break all sliding symmetries, and this cannot happen at finite T , according to the generalized Elitzur theorem of Batista and Nussinov [51]. The sliding symmetries can break spontaneously only at $T = 0$ and in all possible ways, which is reflected in the divergence of the spin structure factor along lines in momentum space.

IV. QUANTUM SPINS AND STRONG-COUPLING EXPANSION

Turning to quantum spins, the situation is fundamentally different because the sliding symmetries are absent from the beginning: To flip one component of the spin, we must combine a π rotation in spin space and the time-reversal operation [54]. The latter, however, involves the complex conjugation, which cannot be constrained to act locally on only one ladder. Essentially, this means that the ladders must couple to each other dynamically by virtual quantum-mechanical processes, which in turn opens the possibility for long-range magnetic ordering even at finite T .

The natural way to understand the dynamical coupling between the ladders is to perform a perturbative expansion around one of the three strong-coupling limits where the above discrete states become true quantum-mechanical ground states. Consider, for example, the limit where the xx and yy couplings, denoted by $K_1^{x(y)}$ and $K_2^{x(y)}$, are much

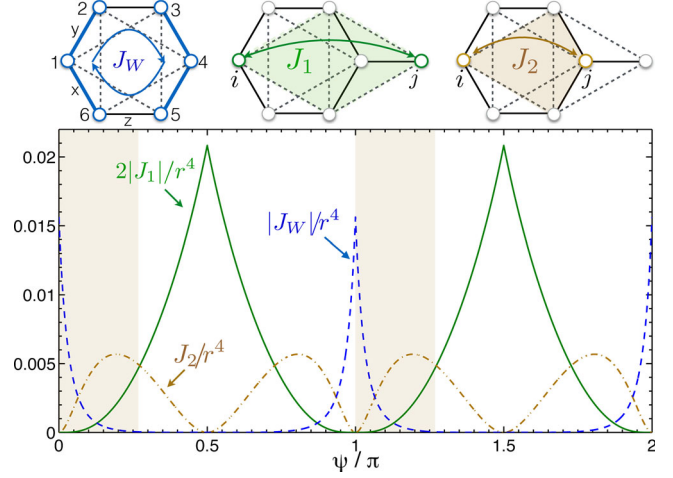


FIG. 5. Top: The three types of virtual processes around the strong-coupling limit $r = 0$ [35]. Bottom: $|J_W|/r^4$, $2|J_1|/r^4$, and J_2/r^4 versus ψ . The shaded strips denote the regions where J_2 competes with J_1 and $J_2 > 2|J_1|$.

smaller than the zz couplings, K_1^z and K_2^z . Let us also parametrize $K_{1,2}^{x(y)} = rK_{1,2}^z$, $K_1^z = \cos \psi$, and $K_2^z = \sin \psi$. For $r = 0$, we have n_{lad} decoupled vertical ladders and $2^{n_{\text{lad}}}$ quantum ground states. Degenerate perturbation theory [35] then shows that the degeneracy is first lifted at fourth order in r via three, loop-four virtual processes that involve (i) only $K_1^{x(y)}$, (ii) only $K_2^{x(y)}$, and (iii) both $K_1^{x(y)}$ and $K_2^{x(y)}$ perturbations; see the top panel of Fig. 5.

The processes (i) give rise to intraladder, six-body terms which are nothing other than the flux operators W_p . As shown by Kitaev [10], these terms can be mapped to the square lattice toric code [57], which has a gapped spin-liquid ground state. Next, the processes (ii) and (iii) give rise to effective, NNN interladder couplings of the form $JS_i^z S_j^z$, where i and j have the same (ii) or different (iii) sublattice unit cell indices; see top panel of Fig. 5. To fourth order in r , the corresponding couplings J_W (i), J_1 (ii), and J_2 (iii) read

$$\begin{aligned}
 J_W &= \frac{-(K_1^x K_1^y)^2 |K_1^z|}{64(|K_1^z| + 2|K_2^z|)^2 (|K_1^z| + 3|K_2^z|) (|K_1^z| + 4|K_2^z|)}, \\
 J_1 &= \frac{(K_2^x K_2^y)^2}{8(|K_1^z| + 2|K_2^z|)^2 (2|K_1^z| + 3|K_2^z|)} \text{sgn}(K_2^z), \\
 J_2 &= \frac{K_1^x K_1^y K_2^x K_2^y}{4(|K_1^z| + 2|K_2^z|)^3} \left[\frac{|K_1^z| + |K_2^z|}{2|K_1^z| + 3|K_2^z|} + \frac{2|K_2^z|}{|K_1^z| + 4|K_2^z|} \right].
 \end{aligned} \tag{3}$$

Note that J_2 is always AFM and competes with J_1 in regions I and III of Fig. 2. We also emphasize that there is no $S_i^z S_j^z$ coupling when i and j belong to NN ladders. This is actually true to all orders in perturbation theory, because of the above nonglobal symmetry H_{xyz} , which

changes the sign of S_z on every second vertical ladder (B and C sites of Fig. 1).

The main panel of Fig. 5 shows the behavior of $|J_W|/r^4$, $2|J_1|/r^4$, and J_2/r^4 as a function of the angle ψ , where the relative factor of 2 between $|J_1|$ and J_2 accounts for their relative contribution to the total classical energy. Close to the exactly solvable points $\psi = 0$ and π , the physics is dominated by the flux terms W_p which, as mentioned above, lead to the gapped toric code QSL [10,57]. The gapless QSL at $r = 1$ is eventually stabilized by off-diagonal processes that necessarily admit states outside the lowest manifold of the $r = 0$ point [58].

The four magnetic phases I–IV of Fig. 2 are all stabilized by J_1 , which, according to Fig. 5, is the dominant coupling in a wide region away from $\psi = 0$ and π . Note that there are also two windows (shaded in Fig. 5) in the beginning of regions I and III where the two interladder terms compete and $2|J_1| < J_2$. This opens the possibility for two more states (the ones favored by J_2) in these regions. This scenario is, however, not confirmed by our ED spectra and spin structure factors (especially for the 32-site cluster which is commensurate with both types of competing phases), showing that these phases are eventually preempted by the QSLs and the phases I and III at higher values of r .

We remark here that the 1-loop formulation of PFFRG delivers the J_2 but not the J_1 processes because, in a diagrammatic formulation of Abrikosov fermions, these processes relate to 3-particle vertex contributions, which require a 2-loop formulation. However, for ψ around 0 and π , where J_1 is small, a 1-loop formulation already yields good agreement.

V. SEMICLASSICAL PICTURE

The magnetic phases of the model can be captured by a standard semiclassical expansion, but this has to go beyond the noninteracting spin-wave level. Indeed, the zero-point energy of the quadratic theory lifts the accidental continuous degeneracy of the problem (selecting the cubic axes for the global direction in spin space, see Ref. [35]), but fails to lift the discrete $2^{n_{\text{lad}}}$ degeneracy (the spectrum has lines of zero modes corresponding to the soft classical twists along individual ladders), and does not deliver a finite spin length, in analogy to several frustrated models [31,50,55,59]. The spurious zero modes are gapped out by spin-wave interactions, leading to the expected anisotropy gap and a finite spin length. The latter (obtained here from a self-consistent treatment of the quartic theory, details of which will be given elsewhere) tracks closely the behavior of the spin length extracted from the ED symmetrized spin structure factor [60] $\tilde{S}(\mathbf{Q})$; see Fig. 3(d). Furthermore, both methods give values that are very close to the classical value of 1/2 inside the magnetic regions, showing that these phases are very robust. The quartic spin-wave expansion is, however, insensitive to

the proximity of the QSLs, most likely due to the first-order character of the transitions.

VI. TRIANGULAR KITAEV POINTS

At $\psi = \pm(\pi/2)$, the system decomposes into two interpenetrating triangular sublattices, where the K_2 coupling plays the role of a NN Kitaev coupling. This problem has been studied for both classical [28,29] and quantum spins [30–32]. The above analysis for the magnetic phases still holds here, the only difference being that the two legs of each ladder decouple, since they belong to different triangular sublattices. The ordering between the legs belonging to the same sublattice stems from the *effective* coupling J_1 , which is the only one surviving at $K_1 = 0$. This coupling connects NNN legs only, leading to 12 states in each sublattice and thus 12^2 states in total, instead of 12 for finite K_1 . The accumulation of such extra states at low energies can be clearly seen in Figs. 3(a) and 3(b) at $\psi = \pm(\pi/2)$. Note that while the ED spectra are broadly independent of system size, significant differences between the two cluster sizes are apparent near $\psi = \pm\pi/2$. These differences, e.g., on the ground-state multiplicity, can be easily traced back to the different point-group symmetry of the two clusters; see a detailed explanation in Ref. [35].

Finally, we point out that the origin of the ordering mechanism at the triangular Kitaev points has also been discussed independently in a recent paper by Jackeli and Avella [31].

VII. DISCUSSION

Charting out the stability region of the Kitaev spin liquid is an extremely relevant endeavor for the synthesis and characterization of new materials. One of the counter-intuitive results of this study is that the frustrating (with respect to long-range magnetic order) NNN coupling K_2 , which has exactly the same anisotropic form and symmetry structure as the K_1 term, destabilizes the Kitaev spin liquid much faster than the nonfrustrating isotropic Heisenberg J_1 coupling. This finding gives a very useful hint in the search of realistic materials that exhibit the Kitaev spin-liquid physics. In $A_2\text{IrO}_3$ materials, for example, the role of the size of the central ion (Na in Na_2IrO_3 or Li in Li_2IrO_3) in mediating the K_2 coupling (see also below) is a key aspect that can be easily controlled by experimentalists [61,62].

On a more conceptual note, the physical mechanism underpinning the magnetic long-range ordering in the present model is a novel example of order by disorder. Unlike many other classical states, here the ordering manifests only for quantum spins and not for classical spins. This striking contrast between classical and quantum spins is even more surprising in light of the fact that all of

these phases have a strong classical character with local pseudospin lengths that are very close to the maximum classical value of $1/2$.

On this issue, we should stress that there is no discrepancy between the very large pseudospin length that we report here and the small length of the magnetic moments extracted from magnetic reflections, e.g., in Na_2IrO_3 [5]. Such an apparent discrepancy can be explained by the value of the g factor, which can be significantly smaller than 2, because the orbital angular momentum is not quenched in strong SOC compounds. For the ideal cubic symmetry, for example, the well-known Landé formula gives $g = 2/3$, and similar values could be expected for lower symmetry.

Let us now elucidate further our main reasons of why the K_2 coupling must play an important role in Na_2IrO_3 , and can be relevant in Li_2IrO_3 and $\alpha\text{-RuCl}_3$.

(i) The superexchange expansion of Ref. [20] shows clearly that the NNN Kitaev coupling is the second largest term in Na_2IrO_3 , with $K_2 \simeq 7\text{--}9$ meV. All other perturbations are at most 1–2 meV, consistent with the numbers given by the large-scale *ab initio* quantum chemistry study of Ref. [15]. The mechanism behind the large magnitude of K_2 in Na_2IrO_3 is physically very clear: It originates from the large diffusive Na ions that reside in the middle of the exchange pathways, and the constructive interference of a large number of four pathways [20].

In Li_2IrO_3 , the K_2 interaction comes from the same mechanism, but it is relatively smaller because of the smaller size of Li ions [26]. Still, as discussed in Ref. [22], this coupling can be important to explain the current experimental evidence in terms of magnetic susceptibility profile, Curie-Weiss temperature, and the relevant range of couplings.

Finally, in $\alpha\text{-RuCl}_3$, the analogous superexchange path is absent, but an appreciable K_2 still arises from the anisotropy of diagonal interactions originated from the interplay between different hopping processes [26]. However, as we pointed out in the Introduction, the second largest coupling in $\alpha\text{-RuCl}_3$ is the anisotropic exchange Γ [15,27]. According to the study of Rau *et al.* [27], a positive Γ seems to compete with K_2 for positive K_1 [26]. However, the situation is still unclear since the Bragg peaks of the states favored by Γ do not reside at the \mathbf{M} points of the BZ found experimentally by Sears *et al.* [13], whereas such Bragg peaks are naturally present in the zigzag phases favored by K_2 , or even by a negative J_1 . So a lot more work is needed to clarify the relative importance of Γ , K_2 and J_1 in $\alpha\text{-RuCl}_3$.

(ii) The K_2 coupling naturally explains the zigzag ordering in Na_2IrO_3 . This phase cannot arise in the original $J_1 - K_1$ model, because this would require an AFM coupling K_1 , whereas it is widely accepted that K_1 is FM and large in magnitude; see, e.g., Ref. [16]. Also, the much smaller Γ terms, which are positive, also favor the zigzag phase and do not compete with K_2 , according to Ref. [27].

(iii) The K_2 coupling can provide, in addition, the basis to resolve the long-standing puzzle of the large AFM Curie-Weiss temperature [2,3,6], without incorporating unrealistically large values of longer-range Heisenberg couplings J_2 and J_3 .

(iv) The recent diffusive x-ray scattering experiments by Chun *et al.* [7] have provided direct evidence for the predominant role of anisotropic, bond-directional interactions in Na_2IrO_3 . In conjunction with the above discussion and the results of Fig. 4, the K_2 term then emerges naturally as the number one anisotropic candidate term that can drive the zigzag ordering and the directional dependence of the scattering found in Ref. [7].

An aspect that remains to be discussed in the context of Na_2IrO_3 is the direction of the magnetic moments which, according to the x-ray scattering data of Chun *et al.* [7], do not point along the cubic axes but along the face diagonals. As discussed above, the K_2 coupling stabilizes the zigzag phase, but it is unable to lock the direction of the moments at the mean-field level due to an infinite accidental degeneracy. The fact that the locking along the cubic axes in the $K_1 - K_2$ model eventually proceeds via a quantum order-by-disorder process (see Ref. [35]) renders this result very susceptible to much smaller anisotropic interactions that can pin the direction of the moments already at the mean-field level. A very small positive anisotropic Γ term can, for example, play such a role and can account for the locking along the face diagonals, as can be seen directly by a straightforward minimization of the classical energy. An alternative scenario involves a competing order-by-disorder effect within a more extended model that includes weak longer-range exchange interactions [26].

ACKNOWLEDGMENTS

We acknowledge the Minnesota Supercomputing Institute (MSI) at the University of Minnesota and the Max Planck Institute for the Physics of Complex Systems, Dresden, where a large part of the numerical computations took place. We are also grateful to R. Moessner, C. Price, O. Starykh, G. Jackeli, Y. Sizyuk, P. Mellado, and M. Schulz for stimulating discussions. I. R. and N. B. P. acknowledge support from NSF Grant No. DMR-1511768. J. R. was supported by the Freie Universität Berlin within the Excellence Initiative of the German Research Foundation. R. T. was supported by the European Research Council through ERC-StG-336012 and by DFG-SFB 1170. S. R. was supported by DFG-SFB 1143, DFG-SPP 1666, and by the Helmholtz association through VI-521. S. R., R. T. and N. B. P. acknowledge the hospitality of the KITP during the program “New Phases and Emergent Phenomena in Correlated Materials with Strong Spin-Orbit Coupling” and partial support by the National Science Foundation under Grant No. NSF PHY11-25915.

- [1] W. Witczak-Krempa, G. Chen, Y. B. Kim, and L. Balents, *Correlated Quantum Phenomena in the Strong Spin-Orbit Regime*, *Annu. Rev. Condens. Matter Phys.* **5**, 57 (2014).
- [2] Y. Singh and P. Gegenwart, *Antiferromagnetic Mott Insulating State in Single Crystals of the Honeycomb Lattice Material Na_2IrO_3* , *Phys. Rev. B* **82**, 064412 (2010).
- [3] Y. Singh, S. Manni, J. Reuther, T. Berlijn, R. Thomale, W. Ku, S. Trebst, and P. Gegenwart, *Relevance of the Heisenberg-Kitaev Model for the Honeycomb Lattice Iridates A_2IrO_3* , *Phys. Rev. Lett.* **108**, 127203 (2012).
- [4] X. Liu, T. Berlijn, W.-G. Yin, W. Ku, A. Tsvelik, Y.-J. Kim, H. Gretarsson, Y. Singh, P. Gegenwart, and J. P. Hill, *Long-Range Magnetic Ordering in Na_2IrO_3* , *Phys. Rev. B* **83**, 220403 (2011).
- [5] F. Ye, S. Chi, H. Cao, B. C. Chakoumakos, J. A. Fernandez-Baca, R. Custelcean, T. F. Qi, O. B. Korneta, and G. Cao, *Direct Evidence of a Zigzag Spin-Chain Structure in the Honeycomb Lattice: A Neutron and X-Ray Diffraction Investigation of Single-Crystal Na_2IrO_3* , *Phys. Rev. B* **85**, 180403 (2012).
- [6] S. K. Choi, R. Coldea, A. N. Kolmogorov, T. Lancaster, I. I. Mazin, S. J. Blundell, P. G. Radaelli, Y. Singh, P. Gegenwart, K. R. Choi, S.-W. Cheong, P. J. Baker, C. Stock, and J. Taylor, *Spin Waves and Revised Crystal Structure of Honeycomb Iridate Na_2IrO_3* , *Phys. Rev. Lett.* **108**, 127204 (2012).
- [7] S. Hwan Chun, J.-W. Kim, J. Kim, H. Zheng, C. C. Stoumpos, C. D. Malliakas, J. F. Mitchell, K. Mehlawat, Y. Singh, Y. Choi, T. Gog, A. Al-Zein, M. M. Sala, M. Krisch, J. Chaloupka, G. Jackeli, G. Khaliullin, and B. J. Kim, *Direct Evidence for Dominant Bond-Directional Interactions in a Honeycomb Lattice Iridate Na_2IrO_3* , *Nat. Phys.* **11**, 462 (2015).
- [8] G. Jackeli and G. Khaliullin, *Mott Insulators in the Strong Spin-Orbit Coupling Limit: From Heisenberg to a Quantum Compass and Kitaev Models*, *Phys. Rev. Lett.* **102**, 017205 (2009).
- [9] J. Chaloupka, G. Jackeli, and G. Khaliullin, *Kitaev-Heisenberg Model on a Honeycomb Lattice: Possible Exotic Phases in Iridium Oxides A_2IrO_3* , *Phys. Rev. Lett.* **105**, 027204 (2010).
- [10] A. Kitaev, *Anyons in an Exactly Solved Model and Beyond*, *Ann. Phys. (Amsterdam)* **321**, 2 (2006).
- [11] R. Schaffer, S. Bhattacharjee, and Y. B. Kim, *Quantum Phase Transition in Heisenberg-Kitaev Model*, *Phys. Rev. B* **86**, 224417 (2012).
- [12] K. W. Plumb, J. P. Clancy, L. J. Sandilands, V. V. Shankar, Y. F. Hu, K. S. Burch, H.-Y. Kee, and Y.-J. Kim, *$\alpha\text{-RuCl}_3$: A Spin-Orbit Assisted Mott Insulator on a Honeycomb Lattice*, *Phys. Rev. B* **90**, 041112 (2014).
- [13] J. A. Sears, M. Songvilay, K. W. Plumb, J. P. Clancy, Y. Qiu, Y. Zhao, D. Parshall, and Y.-J. Kim, *Magnetic Order in $\alpha\text{-RuCl}_3$: A Honeycomb-Lattice Quantum Magnet with Strong Spin-Orbit Coupling*, *Phys. Rev. B* **91**, 144420 (2015).
- [14] Y. Kubota, H. Tanaka, T. Ono, Y. Narumi, and K. Kindo, *Successive Magnetic Phase Transitions in $\alpha\text{-RuCl}_3$: XY-like Frustrated Magnet on the Honeycomb Lattice*, *Phys. Rev. B* **91**, 094422 (2015).
- [15] V. M. Katukuri, S. Nishimoto, V. Yushankhai, A. Stoyanova, H. Kandpal, S. Choi, R. Coldea, I. Rousochatzakis, L. Hozoi, and J. van den Brink, *Kitaev Interactions between $j = 1/2$ Moments in Honeycomb Na_2IrO_3 Are Large and Ferromagnetic: Insights from Ab Initio Quantum Chemistry Calculations*, *New J. Phys.* **16**, 013056 (2014).
- [16] S. Nishimoto, V. M. Katukuri, V. Yushankhai, H. Stoll, U. K. Roessler, L. Hozoi, I. Rousochatzakis, and J. van den Brink, *Strongly Frustrated Triangular Spin Lattice Emerging from Triplet Dimer Formation in Honeycomb Li_2IrO_3* , *arXiv:1403.6698*.
- [17] E. Rastelli, A. Tassi, and L. Reatto, *Non-Simple Magnetic Order for Simple Hamiltonians*, *Physica (Amsterdam)* **97B+C**, 1 (1979).
- [18] J. B. Fouet, P. Sindzingre, and C. Lhuillier, *An Investigation of the Quantum $J_1 - J_2 - J_3$ Model on the Honeycomb Lattice*, *Eur. Phys. J. B* **20**, 241 (2001).
- [19] I. Kimchi and Y.-Z. You, *Kitaev-Heisenberg- $J_2 - J_3$ Model for the Iridates A_2IrO_3* , *Phys. Rev. B* **84**, 180407 (2011).
- [20] Y. Sizyuk, C. Price, P. Wölfle, and N. B. Perkins, *Importance of Anisotropic Exchange Interactions in Honeycomb Iridates: Minimal Model for Zigzag Antiferromagnetic Order in Na_2IrO_3* , *Phys. Rev. B* **90**, 155126 (2014).
- [21] K. Foyevtsova, H. O. Jeschke, I. I. Mazin, D. I. Khomskii, and R. Valentí, *Ab Initio Analysis of the Tight-Binding Parameters and Magnetic Interactions in Na_2IrO_3* , *Phys. Rev. B* **88**, 035107 (2013).
- [22] J. Reuther, R. Thomale, and S. Rachel, *Spiral Order in the Honeycomb Iridate Li_2IrO_3* , *Phys. Rev. B* **90**, 100405 (2014).
- [23] A. Shitade, H. Katsura, J. Kuneš, X.-L. Qi, S.-C. Zhang, and N. Nagaosa, *Quantum Spin Hall Effect in a Transition Metal Oxide Na_2IrO_3* , *Phys. Rev. Lett.* **102**, 256403 (2009).
- [24] J. Reuther, R. Thomale, and S. Rachel, *Magnetic Ordering Phenomena of Interacting Quantum Spin Hall Models*, *Phys. Rev. B* **86**, 155127 (2012).
- [25] H.-S. Kim, V. Vijay Shankar, A. Catuneanu, and H.-Y. Kee, *Kitaev Magnetism in Honeycomb RuCl_3 with Intermediate Spin-Orbit Coupling*, *Phys. Rev. B* **91**, 241110(R) (2015).
- [26] Y. Sizyuk, P. Wölfle, and N. B. Perkins, (to be published).
- [27] J. G. Rau, E. K.-H. Lee, and H.-Y. Kee, *Generic Spin Model for the Honeycomb Iridates beyond the Kitaev Limit*, *Phys. Rev. Lett.* **112**, 077204 (2014).
- [28] I. Rousochatzakis, U. K. Roessler, J. van den Brink, and M. Daghofer, *Z_2 -Vortex Lattice in the Ground State of the Triangular Kitaev-Heisenberg Model*, *arXiv:1209.5895*.
- [29] I. Kimchi and A. Vishwanath, *Kitaev-Heisenberg Models for Iridates on the Triangular, Hyperkagome, Kagome, fcc, and Pyrochlore lattices*, *Phys. Rev. B* **89**, 014414 (2014).
- [30] M. Becker, M. Hermanns, B. Bauer, M. Garst, and S. Trebst, *Spin-Orbit Physics of $j = 1/2$ Mott Insulators on the Triangular Lattice*, *Phys. Rev. B* **91**, 155135 (2015).
- [31] G. Jackeli and A. Avella, *Quantum Order-by-Disorder in Kitaev Model on a Triangular Lattice*, *arXiv:1504.01435*.
- [32] K. Li, S.-L. Yu, and J.-X. Li, *Global Phase Diagram, Possible Chiral Spin Liquid, and Topological Superconductivity in the Triangular Kitaev-Heisenberg Model*, *New J. Phys.* **17**, 043032 (2015).
- [33] G. Khaliullin, *Orbital Order and Fluctuations in Mott Insulators*, *Prog. Theor. Phys. Suppl.* **160**, 155 (2005).

- [34] J. Chaloupka and G. Khaliullin, *Hidden Symmetries of the Extended Kitaev-Heisenberg Model: Implications for the Honeycomb-Lattice Iridates* $A_2\text{IrO}_3$, *Phys. Rev. B* **92**, 024413 (2015).
- [35] See Supplemental Material at <http://link.aps.org/supplemental/10.1103/PhysRevX.5.041035> for auxiliary information and technical details on (i) the classical Luttinger-Tisza minimization in momentum space and the harmonic order-by-disorder process, (ii) our ED study [including the symmetry decomposition of the 12 magnetic states in regions I–II and the definition of $\tilde{S}(\mathbf{Q})$], (iii) momentum space structure factors from PFFRG calculations, and (v) the derivation of Eqs. (3) and (4).
- [36] J. Reuther and P. Wölfle, *$J_1 - J_2$ Frustrated Two-Dimensional Heisenberg Model: Random Phase Approximation and Functional Renormalization Group*, *Phys. Rev. B* **81**, 144410 (2010).
- [37] J. Reuther and R. Thomale, *Functional Renormalization Group for the Anisotropic Triangular Antiferromagnet*, *Phys. Rev. B* **83**, 024402 (2011).
- [38] J. Reuther, D. A. Abanin, and R. Thomale, *Magnetic Order and Paramagnetic Phases in the Quantum $J_1 - J_2 - J_3$ Honeycomb Model*, *Phys. Rev. B* **84**, 014417 (2011).
- [39] J. Reuther, R. Thomale, and S. Trebst, *Finite-Temperature Phase Diagram of the Heisenberg-Kitaev Model*, *Phys. Rev. B* **84**, 100406 (2011).
- [40] This is a degeneracy between three out of the four topological sectors and can appear already for finite systems, depending on the cluster geometry and the corresponding structure of the boundary terms in the fermionic description of the problem [41].
- [41] G. Kells, J. K. Slingerland, and J. Vala, *Description of Kitaev's Honeycomb Model with Toric-Code Stabilizers*, *Phys. Rev. B* **80**, 125415 (2009).
- [42] However, a gap may eventually open at finite K_2 , before the transitions to the magnetically ordered phases.
- [43] E. Fradkin and S. H. Shenker, *Phase Diagrams of Lattice Gauge Theories with Higgs Fields*, *Phys. Rev. D* **19**, 3682 (1979).
- [44] G. Grignani, G. Semenoff, and P. Sodano, *Confinement-Deconfinement Transition in Three-Dimensional QED*, *Phys. Rev. D* **53**, 7157 (1996).
- [45] M. Tsuchiizu and Y. Suzumura, *Confinement-Deconfinement Transition in Two Coupled Chains with Umklapp Scattering*, *Phys. Rev. B* **59**, 12326 (1999).
- [46] S. Mandal, S. Bhattacharjee, K. Sengupta, R. Shankar, and G. Baskaran, *Confinement-Deconfinement Transition and Spin Correlations in a Generalized Kitaev Model*, *Phys. Rev. B* **84**, 155121 (2011).
- [47] For finite systems, these are not true jumps because the transitions involve two states that belong to the same (identity) symmetry sector, leading to a very small level anticrossing.
- [48] G. Baskaran, D. Sen, and R. Shankar, *Spin-S Kitaev Model: Classical Ground States, Order from Disorder, and Exact Correlation Functions*, *Phys. Rev. B* **78**, 115116 (2008).
- [49] Z. Nussinov and J. van den Brink, *Compass Models: Theory and Physical Motivations*, *Rev. Mod. Phys.* **87**, 1 (2015).
- [50] I. Rousochatzakis, J. Richter, R. Zinke, and A. A. Tsirlin, *Frustration and Dzyaloshinsky-Moriya Anisotropy in the Kagome Franciscites $\text{Cu}_3\text{Bi}(\text{SeO}_3)_2\text{O}_2\text{X}$ ($X = \text{Br}, \text{Cl}$)*, *Phys. Rev. B* **91**, 024416 (2015).
- [51] C. D. Batista and Z. Nussinov, *Generalized Elitzur's Theorem and Dimensional Reductions*, *Phys. Rev. B* **72**, 045137 (2005).
- [52] Z. Nussinov and E. Fradkin, *Discrete Sliding Symmetries, Dualities, and Self-Dualities of Quantum Orbital Compass Models and $p + ip$ Superconducting Arrays*, *Phys. Rev. B* **71**, 195120 (2005).
- [53] Z. Nussinov, C. D. Batista, and E. Fradkin, *Intermediate Symmetries in Electronic Systems: Dimensional Reduction, Order out of Disorder, Dualities, and Fractionalization*, *Int. J. Mod. Phys. B* **20**, 5239 (2006).
- [54] By contrast, for the square-lattice compass model [55,56], a π rotation is actually enough (because the model involves only two types of Ising couplings), meaning that sliding symmetries exist also for quantum spins.
- [55] J. Dorier, F. Becca, and F. Mila, *Quantum Compass Model on the Square Lattice*, *Phys. Rev. B* **72**, 024448 (2005).
- [56] B. Douçot, M. V. Feigel'man, L. B. Ioffe, and A. S. Ioselevich, *Protected Qubits and Chern-Simons Theories in Josephson Junction Arrays*, *Phys. Rev. B* **71**, 024505 (2005).
- [57] A. Yu. Kitaev, *Fault-Tolerant Quantum Computation by Anyons*, *Ann. Phys. (Amsterdam)* **303**, 2 (2003).
- [58] K. Phillip Schmidt, S. Dusuel, and J. Vidal, *Emergent Fermions and Anyons in the Kitaev Model*, *Phys. Rev. Lett.* **100**, 057208 (2008).
- [59] G. Khaliullin, *Order from Disorder: Quantum Spin Gap in Magnon Spectra of LaTiO_3* , *Phys. Rev. B* **64**, 212405 (2001).
- [60] The extra factor of 2 in this definition accounts for the fact that there are no correlations between NN ladders for finite systems, due to the symmetry H_{xyz} ; see also Ref. [35].
- [61] G. Cao, T. F. Qi, L. Li, J. Terzic, V. S. Cao, S. J. Yuan, M. Tovar, G. Murthy, and R. K. Kaul, *Evolution of Magnetism in the Single-Crystal Honeycomb Iridates $(\text{Na}_{1-x}\text{Li}_x)_2\text{IrO}_3$* , *Phys. Rev. B* **88**, 220414 (2013).
- [62] S. Manni, Y. Tokiwa, and P. Gegenwart, *Effect of Nonmagnetic Dilution in the Honeycomb-Lattice Iridates Na_2IrO_3 and Li_2IrO_3* , *Phys. Rev. B* **89**, 241102 (2014).